State-Selective Angular and Velocity Distributions of Associatively Desorbing CuF Molecules Determined by CCD Imaging

X. Li, Th. Wach, J. Wanner,* and K. L. Kompa

Max-Planck-Institut für Quantenoptik, Hans-Kopfermann-Strasse 1, D-85748 Garching, Germany

Received: January 15, 1998

The present contribution focuses on a new method of determining state-selective angular and velocity distributions of molecules desorbing from surfaces. It is based on the Doppler-resolved CCD imaging technique, i.e., exciting the molecules with an actively stabilized ring dye laser and imaging the fluorescence by a CCD camera. To analyze the two-dimensional images, a closed form mathematical procedure is used. The technique is applied to associatively desorbing CuF molecules in the reaction of molecular fluorine with copper surfaces. For all rovibrational CuF product levels investigated, the desorbing molecules exhibit a $\cos^n \theta$, $n = 1$, distribution. Assuming that the velocity distributions of the desorbing CuF molecules are Maxwellian, the fitted translational temperatures are equal to the surface temperature within the error limits, proving an indirect reaction mechanism in agreement with previously determined internal state distributions [Bracker, A.; Jakob, P.; Näher, U.; Rüdiger, M.; Sugawara, K.; Wanner, J. *Can. J. Chem.* **1994**, *72* (J. C. Polanyi Special Issue), 643].

I. Introduction

The application of two-dimensional CCD imaging techniques in the field of chemical reaction dynamics significantly simplifies the determination of product velocity, population, and angular momentum alignment by reducing the measurements to one or two geometrical arrangements.[1] Because of its ability to spatially image ions or fluorescence, its application to gas−surface reaction studies can provide state-selective, two-dimensional angular, and velocity distributions of reaction products desorbing from a surface from a single experiment. Several experiments of this kind have been carried out recently.[2,3]

There are essentially two types of CCD imaging techniques, which differ by the determination of the velocity distributions: time-of-flight and Doppler based methods. In the first case molecules moving at different desorption angles and velocities are detected by an expanded laser sheet, from which a two-dimensional CCD image is obtained by imaging the spatial distribution of the molecular ions (REMPI) or fluorescence (LIF) at a certain time delay. From the delay and the distance the molecules travel during the time of flight, one can obtain the velocity distribution, whereas angular distributions can be obtained by measuring the intensity distribution as a function of the desorption angle in a polar coordinate system. Using this method, Menges et al.[3] were able to image state selectively the two-dimensional angular and velocity distributions in the laser-induced desorption of NO from NiO(111) in a single experiment. One particular advantage of this method is, as noted by the authors, that angular distributions for various molecular velocities can be obtained simultaneously.

In the second method, the optical Doppler effect can be used in combination with CCD imaging to determine angular and velocity distributions of desorbing products. The principle of this method is based upon the fact that molecular desorption is unidirectional, which implies that molecules move in the direction along the surface normal. Knowing the laser excitation frequency and the detuning from the exact resonance of the transition, it is possible to transform the intensity distribution in the laboratory frame to velocity distributions of the desorbing molecule. Whereas the time of flight imaging method is mainly applied to pulsed experiments, Doppler imaging can be used for pulsed and cw experiments. Both imaging methods can be state-specific by exciting only one rovibronic transition.

In the present experiment LIF is used in connection with Doppler-resolved CCD imaging. A preliminary account of the Doppler-resolved CCD imaging method has been published previously.[4] The purpose of the current study is to give a detailed description of the refined method. One of the improvements in the present work is the rather unique experimental calibration of the flux-density parameter δ using a Knudsen cell for evaporation of CuF.

Another leads to a thorough treatment of the analysis of the experimental angular and velocity distributions. This has been achieved on the basis of a closed form mathematical formalism.

The method is applied to the F_2/Cu gas−surface reaction. This system has been investigated thoroughly in terms of internal product-state distributions in our laboratory.[5] The angular and velocity distributions in this study completes the product-state analysis of CuF molecules desorbing associatively from Cu surfaces. Hence the fluorine/copper reaction system is one of the rare examples of a gas−surface reaction for which the complete product-state analysis could be obtained by means of a single optical experiment.

II. Experimental Setup

The experimental setup is depicted in Figure 1a. A polycrystalline copper sample, composed of isotopically purified ^{63}Cu (99.6% purity) or a copper (111) single-crystal surface with natural isotopic abundance (Lamprecht), heated to ∼980 K is dosed by a molecular fluorine beam. To define the reaction region and to reduce thermal background radiation of the sample heater, the surface is covered with a tantalum aperture with an

10.1021/jp980794s CCC: $15.00
Published on Web 06/24/1998

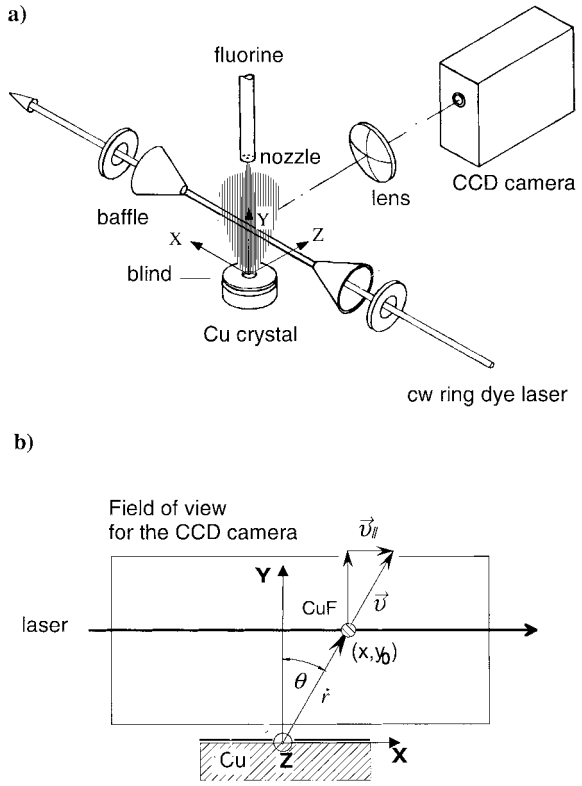

Figure 1. (a) Experimental setup; (b) the three-dimensional coordinate system of the current experiment.

opening of 2 mm in diameter. The fluorine beam (99.999% purity) typically expands at a flow of 2.5×10^{-3} mbar L s^{-1} from a platinum/iridium nozzle with an orifice of 0.2 mm. The fluorine flow is controlled by a mass flow meter.

Rotationally resolved transitions of the C−X band system of the desorbing CuF molecules are excited using an actively stabilized, tunable cw ring dye laser with coumarin 102 (Spectra Physics 380D), pumped by a Kr^+ ion laser (Spectra Physics 2080-KR-V). In single-mode operation typically a power of about 150 mW with a bandwidth of several megahertz is used. The laser wavelength is controlled by a wavemeter[6] of the Hall and Lee type[7] with an accuracy of about 500 MHz and a 1.996 GHz scanning etalon. The laser beam is steered parallel to the copper surface at a typical distance of $y = 15$ mm adjusted with an accuracy of ±0.2 mm. Laser stray light at the entrance and exit windows (CaF_2, AR coated for 500 nm) is suppressed by a set of light baffles mounted inside the chamber. The photon detection system is positioned outside the chamber behind a third window (BK7 with broad-band AR coating), perpendicular to the laser beam and the surface normal. It is composed of a commercial camera lens (85 mm focal length, 70 mm aperture), a set of filters, and a CCD camera. For this study an image-intensified CCD camera (LaVision, "Flame Star") in slow scan mode with a 12-bit dynamic range is used. The two interference filters transmitting at $\lambda_1 < 700$ nm, $\lambda_2 < 543$ nm are mounted between the CCD camera and the camera lens in order to reduce the background radiation of the heater and retain a maximum transmission for the fluorescence light. To maximize the fluorescence signal by choosing the optimum plane of polarization a Fresnel rhomb is inserted in the laser beam.

Most of the imaging experiments are carried out using a ^{63}Cu polycrystalline sample owing to the better spectral resolution of the isotopically pure ^{63}CuF molecule. Experiments are also done using a Cu(111) single-crystal surface with natural isotopic abundance. Additionally a reference experiment is carried out in which CuF evaporates from a Knudsen cell made from copper. According to the work of Ehlert and Wang,[8] the oven is filled with a CuF_2/Cu powder mixture. The copper powder is added to suppress etching of the oven. The device is heated to 800−1000 K to generate CuF. The cover of this oven is made from a 0.5 mm thin silver metal sheet with an orifice of 0.5 mm in diameter to realize a well-defined point source for evaporation.

III. Two-Dimensional CCD Imaging of the Fluorescence of Desorbing CuF Molecules

1. Principles of Doppler-Resolved CCD Imaging Technique. CCD imaging offers the intrinsic advantage that the spatial fluorescence distribution can be monitored. Using the optical Doppler effect one can measure state-selective angular and velocity distributions of molecules desorbing reactively from a surface or evaporating from a Knudsen cell, provided that there is no overlap with other transitions. The principles of such measurements are outlined in the following.

At a fixed laser frequency, which is shifted by $\Delta\nu$ from the resonance frequency ν_0 of a particular rovibronic transition, owing to the optical Doppler effect, only those molecules are excited, which have a proper velocity component $v_{\parallel}$ parallel to the laser beam as given by

$$v_{\parallel} = c\frac{\Delta\nu}{\nu_0} \tag{1}$$

Since

$$v_{\parallel} = v \cdot \sin\theta \tag{2}$$

the velocity distribution of the desorbing molecules, which are superimposed by the angular distributions, can be deduced from the fluorescence intensity patterns as shown in Figure 2.

In Figure 2 we present CCD images that were obtained by tuning the laser in steps of 0.5 GHz (from red to blue) across the Doppler-broadened line profile of the CuF C−X (0,0) Q(57) transition. The near-resonant excitation condition occurs in Figure 2c. It can be seen from Figure 2a−d that the fluorescence pattern in the horizontal direction broadens with increasing laser detuning. This is easy to understand since, according to eq 2,

$$\frac{dv}{v} = -\frac{\cos\theta}{\sin\theta} \cdot d\theta \tag{3}$$

Approaching the resonance ($\sin\theta \rightarrow 0$), a small change in the desorption angle $d\theta$ will result in a large velocity dv variation, and the velocity distribution is imaged in a smaller desorption angle $\Delta\theta$. When the laser is tuned to exact resonance with the transition, $\nu = \nu_0$, a Doppler-free condition is fulfilled and the velocity distribution cannot be imaged.

2. Angular and Velocity Distributions of the Desorbing CuF Molecules from a Surface. In Figure 1b the three-dimensional coordinates with the origin at the center of the circular surface area are visualized. The laser is assumed to propagate along the *X*-axis. Since the effective laser diameter (typically around 100 μm) is much smaller than the distance (about 15 mm) between the laser beam and the surface, the fluorescence intensity $I_{fl}(x, y, z)$ in the three-dimensional space is approximated by $I_{fl}(x, y, z = 0) = I_{fl}(x, y)$ in the two-dimensional plane.

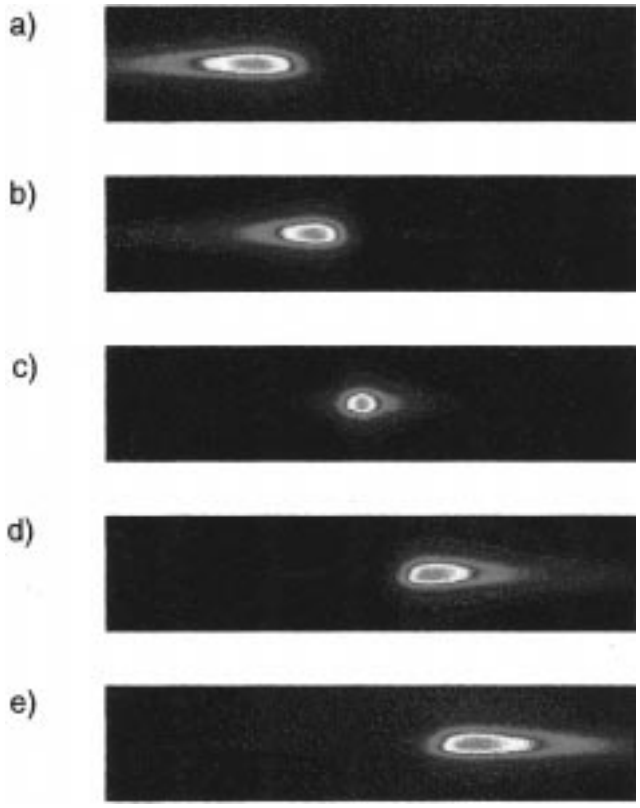

Figure 2. CCD images of the fluorescence of the CuF C−X (0,0) Q(57) transition at different laser frequencies. The laser is tuned to about (a) −1.0 GHz; (b) −0.5 GHz; (c) 0.0 GHz; (d) 0.5 GHz; (e) 1.0 GHz from the molecular resonance. The surface temperature T_S is 1000 K.

The number of molecules, dN, leaving the surface area element, dσ = dxdz, with a velocity between v and $v + dv$ into a solid angle element, dω, which axis is at an angle θ, with respect to the normal of surface is given by

$$\mathrm{d}N = n_0 f(v)\frac{\mathrm{d}\omega}{2\pi} v \cos^n\theta \cdot \mathrm{d}\sigma \mathrm{d}t \mathrm{d}v \quad (4)$$

where n_0 is the number density of the desorbing molecules at the surface and $f(v)$ the normalized speed distribution of the molecules. In the above formula it is assumed that the angular distribution could be described by a $\cos^n\theta$ term, and the speed distribution is independent of the desorption angle θ.

Taking into account the effective size of the desorption area, the total number of molecules leaving the surface area per unit time into a solid angle element dω (molecular flux into dω) is equal to

$$I(\theta, v)\,\mathrm{d}\omega = \frac{\mathrm{d}N}{\mathrm{d}t} = \int\int_R \frac{n_0}{2\pi} f(v) \cdot v \cdot \cos^n\theta\, \mathrm{d}v \mathrm{d}\sigma \mathrm{d}\omega \quad (5)$$

The number density is

$$n(r, \theta, v) = \frac{I(\theta, v)\,\mathrm{d}\omega}{\mathrm{d}V} = \int\int_R \frac{n_0}{2\pi} f(v) \cdot \cos^n\theta\, \mathrm{d}v \frac{\mathrm{d}\sigma}{r^2} \quad (6)$$

To obtain state-selective angular distributions, the laser frequency is rapidly scanned over the Doppler profile of the transition. All molecules are sampled irrespective of their velocities. If we use dM to specify the detection area in the yz-plane, since dω = dM·cos θ/r^2, one obtains for the detection of molecular flux

$$f_{\mathrm{ang}}\,\mathrm{d}M = \int_0^\infty I(\theta, v)\,\mathrm{d}v \cdot \frac{\cos\theta}{r^2} \cdot \mathrm{d}M = v_w \int\int_R \frac{n_0}{2\pi} \cos^{n+1}\theta \frac{\mathrm{d}\sigma}{r^2} \cdot \mathrm{d}M \quad (7)$$

where v_w is the most probable speed of the molecule. For the detection of molecular density one gets

$$f_{\mathrm{ang}}\,\mathrm{d}M = \int_0^\infty n(r, \theta, v)\,\mathrm{d}v \cdot \mathrm{d}M = \int\int_R \frac{n_0}{2\pi} \cos^n\theta \frac{\mathrm{d}\sigma}{r^2} \cdot \mathrm{d}M \quad (8)$$

Combining the above two equations, we obtain the following general relation

$$f_{\mathrm{ang}}\,\mathrm{d}M \propto \int\int_R \frac{n_0}{2\pi} \cos^{n+\delta}\theta \cdot \frac{\mathrm{d}\sigma}{r^2} \cdot \mathrm{d}M \quad (9)$$

where δ can take any value between 0 and 1 depending on the excitation condition. For density detection we have $\delta = 0$; for flux detection $\delta = 1$ (for a detail discussion, see section IV).

When measuring molecular velocity distributions, the laser is stabilized at a given frequency. At a given (r, θ), only those molecules from the infinitely small surface area element dσ can absorb a laser photon, for which the Doppler-shifted frequency falls within the natural line width of the molecule. On the basis of eqs 1, 2 and 5, 6, and assuming a Maxwellian velocity distribution,

$$f(v) \propto v^2 \cdot \exp\left(-\frac{mv^2}{2kT_{\mathrm{trans}}}\right) \quad (10)$$

one obtains the distribution of excited CuF molecules along the direction of the laser

$$f_{\mathrm{vel}}\,\mathrm{d}M \propto \int\int_R \frac{n_0}{2\pi} \cos^{n+\delta}\theta \cdot \frac{v_{||}^{2+\delta}}{\sin^{3+\delta}\theta} \cdot \exp\left(-\frac{mv_{||}^2}{2kT_{\mathrm{trans}}\sin^2\theta}\right) \frac{\mathrm{d}\sigma}{r^2} \cdot \mathrm{d}v_{||}\mathrm{d}M \quad (11)$$

Knowing $\Delta\nu$ and ν_0 and thus $v_{||}$, it is possible to obtain the translational temperature by fitting of the experimental profile.

The accuracy of the translational temperature determination depends on how well the velocity distribution profile f_{vel} is determined. According to eq 3, the velocity profile f_{vel} could be deduced with higher accuracy when the laser is tuned out of resonance of the transition. Consequently the translational temperature determination is usually performed at out-of-resonance conditions.

3. Spectroscopic Features of the CuF C−X Transition in the Deconvolution of CCD Images. The CuF molecule has low-lying electronic states that can be excited from the ground state in the visible spectral region.[9] Among the various electronic transitions the $C^1\Pi - X^1\Sigma^+$ band system has a high electronic transition probability.[10−12] The corresponding (0,0) Q branch band head is located at 493.35 nm. For the rovibronic transitions with $v' = v''$, the Franck−Condon factors approach unity.[13] The line positions of the C−X band system and the corresponding molecular constants for the ^{63}CuF isotope have been revised recently in our group.[14] The rotational spectra of the ^{65}CuF isotope and the electronic isotope shift have been observed.[15]

The hyperfine splitting (hfs) in the $C^1\Pi$ state leads to an additional structure of the high-resolution spectra. This originates from the magnetic dipole and electric quadruple interactions of the Cu nucleus ($I = {}^3/_2$) and the F nucleus ($I = {}^1/_2$) with the molecular rotation. According to previous measurements,[16] the interaction of the Cu nucleus is much stronger than that of the F nucleus. Hence, each rovibronic line splits into a quartet (Cu spin) superimposed by a doublet (F spin).

The hyperfine splitting in the CuF $C^1\Pi$ state decreases with increasing molecular rotation. While the hfs splitting is too small for transitions with high rotational quantum numbers to be resolved in the CCD images (see Figure 2c), it could be partially resolved for transitions with low rotational quantum numbers (see upper panel of Figure 5).

The significant hyperfine splitting in the CuF C−X transition complicates the deconvolution process of the velocity distribution from the experimental intensity profiles, because contributions from different velocity groups (corresponding to the four hyperfine structure components) to the detector at (r, θ) are possible. Using nonlinear least-squares fitting procedures to directly obtain the translational temperature, it is rather ineffective because the fitted results strongly depend on the initial parameters. Instead, the translational temperature is obtained by minimizing the difference of the calculated and the experimental intensity profiles using the translational temperature as an adjustable parameter.

In order to determine the translational temperature, it is necessary to know the exact detuning of the laser from the resonance frequency and the relative intensities of the different hyperfine structure components. Thus the velocity distribution experiments are carried out in two separate steps. In the first step the laser is tuned to near resonance with the transition. The spatial fluorescence distribution is recorded using the CCD camera. Sine the intensity profile is rather sensitive to the laser frequency at resonance, it is possible to obtain the laser frequency (within a few megahertz) by minimizing the difference between the calculated and the experimental profiles. The relative intensities of the different hyperfine components are also deduced from the calculation; in the second step the laser is tuned out of resonance by a certain amount, typically 500 MHz in the current experiment. Using the translational temperature as an adjustable parameter, the intensity profile is optimized until the difference approaches a minimum between the calculated and the experimental intensity profiles.

Typically Q branches are used to record CCD images because of their larger intensities compared with the P and R branches. Since the detection sensitivity of CCD pixels is not exactly uniform, the experimental images are normalized with a reference picture from the manufacturer.

IV. Results and Discussion

The numerical procedure of section III.2 requires a correct value for δ, which needs to be incorporated into eqs 9 and 11. From the point of the physics, one addresses a rather general problem associated with product-state distribution measurements by laser techniques, namely, whether flux ($\delta = 1$) or density ($\delta = 0$) is probed. This particular issue has received ongoing attention since for most experiments δ cannot be obtained experimentally but has to be deduced from theoretical considerations. An excellent description of this topic is given by Hefter and Bergmann.[17] The experiments presented in our study offer a rather unique opportunity for the determinion of δ as described below.

1. Angular Distributions. Scanning the laser across the whole Doppler-broadened transition and simultaneously recording the spatial fluorescence using the CCD camera, angular distribution images have been obtained. A typical angular distribution image from CuF desorbing from the polycrystalline copper surface is shown in the upper panel of Figure 3 for the (0,0) Q(57) transition. After normalizing the CCD image with the reference picture, the experimental angular distribution profile is obtained. This is visualized in the lower panel of Figure 3. The experimental angular distribution profile is then fitted to eq 9 using a linear least-squares fitting procedure. The best match $n + \delta$ value is calculated to about 1.54 ± 0.10. The accuracy is estimated to be around 0.10 owing to fluctuations in the laser power as well as inaccuracies in the transformation from CCD pixels to laboratory coordinates. The calculated angular distribution using the fitted results is depicted together with the experimental data in Figure 3, lower panel.

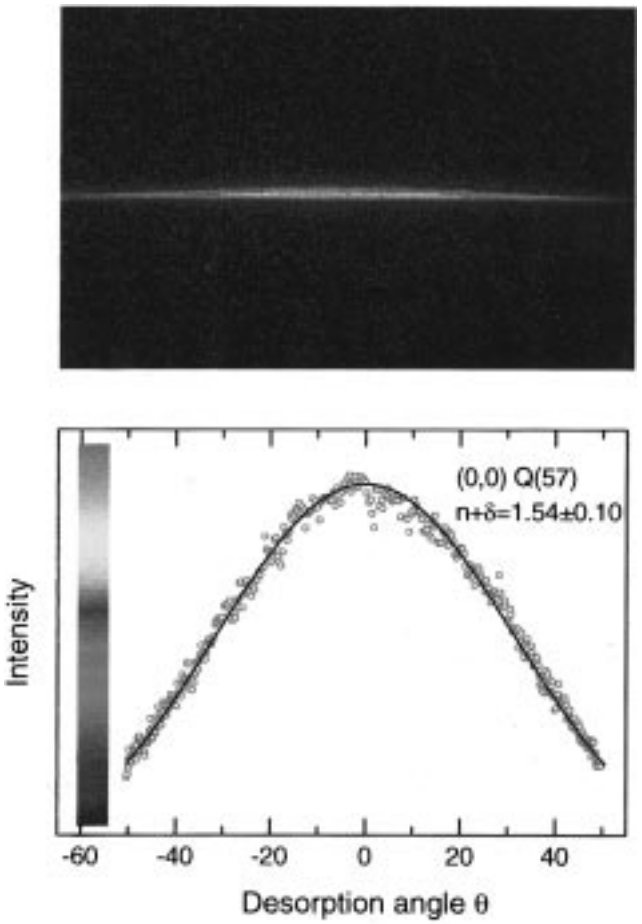

Figure 3. Upper panel: CCD image of the CuF C−X (0,0) Q(57) transition obtained by scanning the laser over the whole Doppler profile. Lower panel: Horizontal intensity profile for the above CCD image along the laser axis. The experimental angular distribution is depicted in open circles and the calculated profile by a solid line.

Once the $n + \delta$ value has been determined, in order to deduce the value of n, it is necessary to know the value of δ. Under the current experimental conditions, the residence time of the molecules within the field of view of the CCD camera is much larger than the lifetime of the CuF molecule (about 0.6 μs). From a theoretical point of view, for weak excitation, molecular density ($\delta = 0$) is expected. For strong excitation, molecular flux ($\delta = 1$) should be detected. If the excitation falls within weak and strong excitation, the value of δ may vary from 0 to 1.[17]

The experimental determination of δ was carried out with the Knudsen cell described in the experimental section. It is well-established that molecules emerging from such an oven

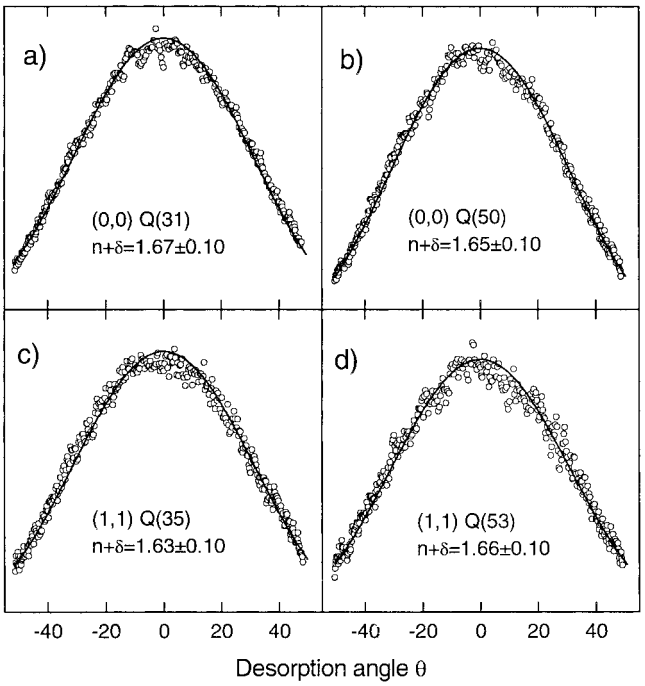

Figure 4. Angular distribution profiles for CuF molecules desorbing from a polycrystalline copper surface. The images are recorded with the (a) (0,0) Q(31); (b) (0,0) Q(50); (c) (1,1) Q(35); (d) (1,1) Q(53) transitions. The calculated angular distributions with the results obtained from a general linear least-squares fitting program are also depicted.

TABLE 1: Angular Distribution ($n + \delta$) Values Determined by the Procedure Described in the Text for CuF Molecules Emerging from a Knudsen Cell and Those Desorbing Associatively from a Polycrystalline Copper Surface

transition	$n + \delta$	transition	$n + \delta$
Knudsen Cell $T_c \approx 990$ K			
(0,0) Q(57)	1.52 ± 0.10	(0,0) Q(13)	1.54 ± 0.10
Etching of Polycrystalline Copper $T_s \approx 990$ K			
(0,0) Q(31)	1.67 ± 0.10	(1,1) Q(35)	1.63 ± 0.10
(0,0) Q(50)	1.65 ± 0.10	(1,1) Q(39)	1.78 ± 0.10
(0,0) Q(57)	1.54 ± 0.10	(1,1) Q(53)	1.66 ± 0.10

exhibit a $\cos^n \theta$, $n = 1$, angular distribution and a Maxwellian velocity distribution corresponding to the oven temperature.[18] Hence, to obtain a value for δ, the state-selective angular distribution of CuF molecules evaporating from the oven was measured. For these measurements the (0,0) Q(57) transition was employed. The obtained angular distribution value, $n + \delta$, is listed in Table 1. The δ value obtained from the Knudsen cell measurement is about 0.5. This means that the current experiment is performed under conditions of detection that fall between flux and density measurements.

Following this calibration the fluorescence of several other ^{63}CuF transitions corresponding to product states $v' = 0$, $J' = 31$, 50, 57 and $v' = 1$, $J' = 35$, 39, 53 was imaged for the etching of polycrystalline copper by fluorine. In Figure 4 we present the angular distribution profiles for a few examples. All resulting $n + \delta$ values are listed in Table 1. The variations in $n + \delta$ may be attributed to changes in the laser power. Subtracting δ, all n values in Table 1 are close to 1. Consequently the CuF molecules produced by reactive etching desorb with a $\cos^n \theta$, $n = 1$ distribution, independent of the rovibrational product level.

Similar measurements were also carried out with the Cu (111) single crystal. The obtained results show an identical behavior but were not elaborated in detail.

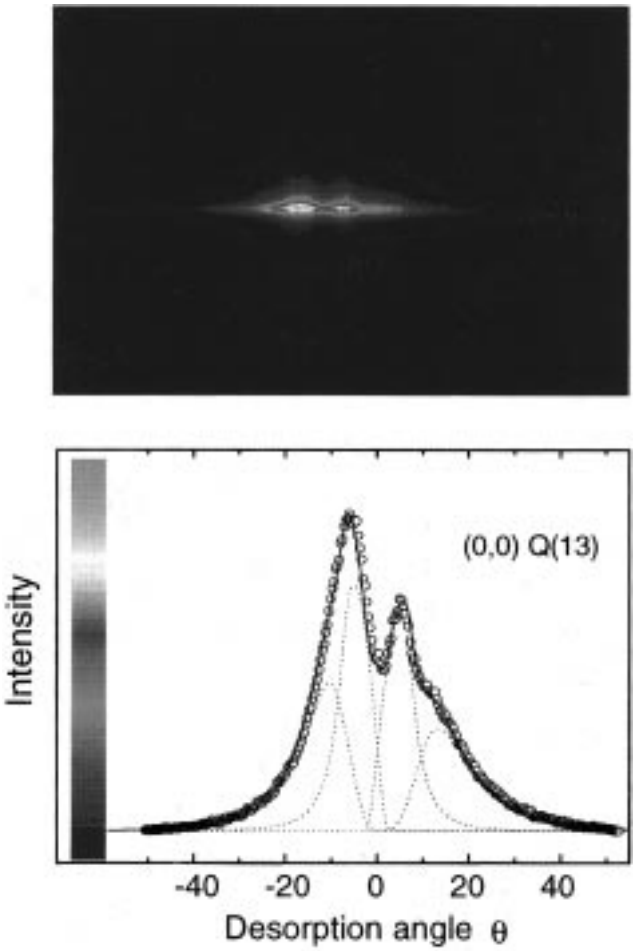

Figure 5. Upper panel: CCD image recorded by exciting the CuF C−X (0,0) Q(13) transition. The laser is nearly resonant with one hyperfine structure (hfs) line. Lower panel: In the corresponding horizontal intensity profile the open circles refer to the experimental data, the solid curve refers to the fitted result, and the dotted curves refer to the contributions from the four hfs components.

2. Velocity Distributions. The translational temperature of CuF molecules desorbing associatively from solid copper is determined in two separate steps as described in section III.3. In the upper panel of Figure 5, we present the CCD image for the laser being tuned to near resonance with the (0,0) Q(13) transition. The four partially resolved hfs components are clearly seen. The experimental intensity profile is shown with open circles in the lower panel of Figure 5. Using the laser frequency and the relative intensities as an adjustable parameter, the intensity profile is calculated using eq 11. The optimum intensity profile $f_{vel}(r, \theta)$ is shown in the lower panel of Figure 5 as a solid line. The velocity distributions from the four hfs lines are shown as dotted curves. The hfs splittings are taken from the literature.[16,19]

In the upper panel of Figure 6, the laser is tuned to the red by 0.5 GHz. The image pattern is broadened, and the four hfs components overlap with each other. The corresponding intensity profiles $f_{exp}(r, \theta)$ are visualized in the lower panel Figure 6 as open circles. Using the parameters obtained from the lower panel of Figure 5 and the angular distribution from the measurement described in the previous section, the intensity profile is calculated using eq 11, and the difference between the two is compared. Using the translational temperature as an adjustable parameter, iterations are performed until the difference between the two profiles is minimized. The obtained translational temperature is about 970 K. The accuracy of the

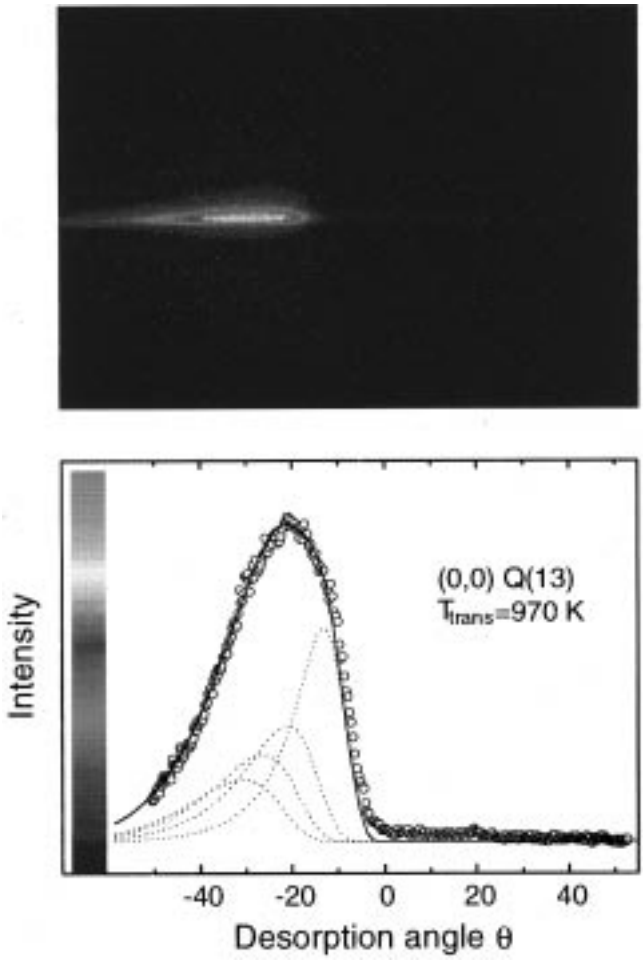

Figure 6. Upper panel: CCD image corresponding to a laser frequency that is shifted by 500 MHz with respect to the measurement shown in the upper panel of Figure 5. The hfs components are largely overlapped. Lower panel: From the horizontal intensity profile the translational temperature was determined by a fit as described in the text.

TABLE 2: For a Selection of the Transitions from Table 1, the Translational Temperatures of the CuF Molecules Desorbing Associatively from Polycrystalline Copper Determined by Deconvoluting CCD Images According to the Text

transition	T_{trans} (K)	transition	T_{trans} (K)
(0,0) Q(31)	960	(1,1) Q(39)	960
(0,0) Q(50)	980	(1,1) Q(53)	950
(0,0) Q(57)	1010		

determined translational temperature is about 80 K, which is mainly due to inaccuracies of the angular distribution as well as due to the frequency determination. The fitted value falls within the error limits of the measured surface temperature.

Using the same procedure, the fluorescence for a number of transitions listed in Table 1 was also imaged. Using the known angular distributions, the velocity distribution profiles were fitted in an iterative procedure. The obtained translational temperatures are shown in Table 2. They all correspond to the surface temperature within the error limit for the product levels $v' = 0$, $J' = 13$, 31, 50, 57 and $v' = 1$, $J' = 39$, 53.

A second set of measurements (not listed in Table 2) was carried out with a Cu single-crystal surface with a defined orientation (111). In this case owing to a more significant overlap only few transitions in comparison with the etching of the isotopically purified sample could be used for a determination of state-selected angular and velocity distributions: (0,0) Q(57) and (1,1) Q(55). The intensity profiles and the corresponding fits according to eq 11 are of the same quality as the data displayed in Figures 5 and 6.

In summary the results of the state-selected velocity distributions of CuF in the reaction of F_2 with a polycrystalline Cu sample and a Cu(111) single-crystalline surface demonstrate that the calculated temperature parameter T_{trans} agrees with the surface temperature within the error limits, independent of the rovibrational product level.

V. Conclusions

A new method for determining state-selective angular and velocity distributions by two-dimensional imaging of laser-induced fluorescence based on the optical Doppler effect is described. The technique is applied to CuF molecules associatively desorbing from the F_2/Cu surface reaction. The analysis of the experimental data show that the CuF molecules desorb from the surface with a $\cos^n \theta$, $n = 1$ distribution, with a translational temperature that agrees with the surface temperature within the error limits, independent of the rovibrational levels. This, in addition to previous internal product distribution analysis,[5] is a further proof of an indirect reaction mechanism. Hence, the steps of the F_2/Cu system may be addressed to as

$$^1/_2F_2(g) + Cu(s) \rightarrow F(ad) + Cu(s) \rightarrow CuF(ad) \rightarrow CuF(g)$$

The absence of a product translational heating as verified in this study is consistent with the previously noted absence of vibrational heating. This indicates the absence of a barrier beyond the desorption potential. By the application of microscopic reversibility, this is equivalent with the absence of a barrier for adsorption of CuF from solid copper.[5] Hence, the associative CuF desorption is a strict example of nonactivated desorption. This is surprising since the exoergicity of the reaction would allow a more direct pathway.

Acknowledgment. This study was performed within the context of the Sonderforschungsbereich 338. We thank H. Schröder for pointing out the potential of CCD imaging, G. Hall for a stimulating discussion, and A. Steyer for technical support. We are also obliged to S. Wurm and C. R. Vidal for critical comments on the manuscript.

References and Notes

(1) Houston, P. L. *Acc. Chem. Res.* **1995**, *28*, 453−460. Houston, P. L. *J. Phys. Chem.* **1996**, *100*, 12757.
(2) Corr, D.; Jacobs, D. C. *Rev. Sci. Instrum.* **1992**, *63*, 1969.
(3) Menges, M.; Baumeister, B.; Al-Shamery, K.; Freund, H.-J.; Fischer, C.; Andresen, P. *Surf. Sci.* **1994**, *316*, 103.
(4) Sugawara, K.; Sun, W.; Wach, Th.; Wanner, J. *Ber. Bunsen-Ges. Phys. Chem.* **1995**, *99*, 1357.
(5) Bracker, A.; Jakob, P.; Näher, U.; Rüdiger, M.; Sugawara, K.; Wanner, J. *Can. J. Chem.* **1994**, *72* (J. C. Polanyi Special Issue), 643.
(6) Näher, U. Diploma Thesis, Technische Universität München, (1990); MPQ Report, 1990, No. 149.
(7) Hall, J. L.; Lee, S. A. *Appl. Phys. Lett.* **1976**, *29*, 367.
(8) Ehlert, T. C.; Wang, J. S. *J. Phys. Chem.* **1977**, *81*, 2069.
(9) Steele, R. E.; Broida, H. P. *J. Chem. Phys.* **1978**, *69*, 2300.
(10) Ahmed, F.; Barrow, R. F.; Chojnicki, A. H.; Dufour, C.; Schamps, J. *J. Phys. B: At. Mol. Phys.* **1982**, *15*, 3801.
(11) Schamps, J.; Delaval, J. M.; Faucher, O. *Chem. Phys.* **1990**, *145*, 101.
(12) Chen, X. R.; Wagemann, K.; Wanner, J.; Brenig, W.; Küchenhoff, S. *Surf. Sci.* **1989**, *224*, 570.

(13) Schwenz, R. W.; Parson, J. M. *J. Chem. Phys*. **1980**, *73*, 259.
(14) Jakob, P.; Sugawara, K.; Wanner, J. *J. Mol. Spectrosc*. **1993**, *160*, 596.
(15) Chen, X. R.; Wagemann, K.; Wanner, J. Unpublished results.
(16) Jakob, P.; Sugawara, K.; Wanner, J.; Bath, A.; Tiemann, E. *Can. J. Phys.* **1994**, *72* (G. Herzberg Special Issue), 1087.
(17) Hefter, U.; Bergmann, K. In *Atomic and Molecular Beam Methods*; Scoles, G., Bassi, D., Buck, U., Lainé, D., Eds.; Oxford University Press: New York, Oxford, 1988; Vol. 1, p 193ff.
(18) Goodman, F. O.; Wachman, H. Y. *Dynamics of Gas-Surface Scattering*; Academic Press: New York, San Francisco, London, 1976; p 23.
(19) Wach, Th. Ph.D. Thesis, Ludwig-Maximilians-Universität München, 1995; MPQ Report, 1995, No. 200.